Membrane Tether Formation from Outer Hair Cells with Optical Tweezers

Zhiwei Li,* Bahman Anvari,* Masayoshi Takashima,† Peter Brecht,* Jorge H. Torres,* and William E. Brownell†
*Department of Bioengineering, Rice University, Houston, Texas 77251 USA; and †Bobby R. Alford Department of Otorhinolaryngology and Communicative Sciences, Baylor College of Medicine, Houston, Texas 77030 USA

ABSTRACT Optical tweezers were used to characterize the mechanical properties of the outer hair cell (OHC) plasma membrane by pulling tethers with 4.5-μm polystyrene beads. Tether formation force and tether force were measured in static and dynamic conditions. A greater force was required for tether formations from OHC lateral wall (499 $\pm$ 152 pN) than from OHC basal end (142 $\pm$ 49 pN). The difference in the force required to pull tethers is consistent with an extensive cytoskeletal framework associated with the lateral wall known as the cortical lattice. The apparent plasma membrane stiffness, estimated under the static conditions by measuring tether force at different tether length, was 3.71 pN/μm for OHC lateral wall and 4.57 pN/μm for OHC basal end. The effective membrane viscosity was measured by pulling tethers at different rates while continuously recording the tether force, and estimated in the range of 2.39 to 5.25 pN·s/μm. The viscous force most likely results from the viscous interactions between plasma membrane lipids and the OHC cortical lattice and/or integral membrane proteins. The information these studies provide on the mechanical properties of the OHC lateral wall is important for understanding the mechanism of OHC electromotility.

INTRODUCTION

Cochlear outer hair cells (OHCs) are one of the two mammalian sensory receptor cells of hearing. Hair cells get their name from the fact they have thin cellular projections (stereocilia) at their apical end. The OHCs are cylindrically shaped with a diameter of ~9 μm and lengths that vary between 15 and 90 μm, depending on their location in the cochlea. They have three cellular regions (the flat apex, hemispheric base, and lateral wall) that perform different functions. The stereocilia at the apex of the cell convert mechanical energy of sound into electrical energy. Synaptic structures at the base of the cell convert electrical energy into chemical energy by modulating the release of neurotransmitters that activate the 8th nerve fibers contacting the cell. The lateral wall is believed to be responsible for electrically induced length changes known as electromotility (Brownell et al., 1985). Electromotilty is unique to OHCs, and no other cell is known to change its length in response to electrical stimulation.

Sound causes the organ of Corti to vibrate and OHCs sense the vibration through the bending of their stereocilia. The resulting change in the OHCs transmembrane potential drives electromotility. The OHCs length change exert a force against the tectoral membrane, amplifying the basilar membrane vibration and refining the sensitivity and frequency selectivity of cochlear mechanical vibrations (Brownell et al., 1985, 2001; Ashmore, 1987; Brownell, 1990; Dallos and Corey, 1991; Holley, 1996).

The mechanism responsible for OHC electromotility is unknown. A popular hypothesis is that electromotility results from conformational change of motor molecules in the lateral wall leading to changes in lateral wall surface area (Santos-Sacchi, 1993; Isawa, 1993, 1994). The OHC lateral wall is a 100-nm thick trilaminate structure consisting of the plasma membrane (PM), cortical lattice (CL), and subsurface cisternae (SSC) (Fig. 1) (Brownell and Popel, 1998; Brownell et al., 2001). Transmission electron microscopy reveals that the plasma membrane has nanometer scale ripples (Dieler et al., 1991; Holley, 1996) that may provide the necessary membrane reservoir for cell length changes. An alternative hypothesis for electromotility is that changes in transmembrane potential alter the curvature of nanoscale ripples (Raphael et al., 2000).

The cortical lattice, sandwiched between SSC and PM, is composed of cytoskeletal microdomains of parallel actin filaments cross-linked with spectrin. Ultrastructural studies have revealed the presence of pillars ~35 nm in length linking the cortical lattice to the plasma membrane (Arima et al., 1991; Holley, 1992). The function of the pillar is probably the mechanical coupling of PM to CL through which the force generated by the motor mechanism can be transferred to CL and SSC. The SSC is composed of concentric layers of flattened membranes that form the innermost layer of the lateral wall. It shares common features with both Golgi apparatus and endoplasmic reticulum (Pollice and Brownell, 1993). The mechanics of the lateral wall and plasma membrane have been previously studied using micropipette aspiration (Sit et al., 1997; Spector et al., 1998a,b; Oghalai et al., 1998; Morimoto et al., 2002).

An important question is how the membrane motor mechanism directs its force to induce electromotility. The mechanical properties of each of the lateral wall layers and the force coupling among them are central to this question. Additionally, the mechanical properties are important pa-

Submitted April 23, 2001, and accepted for publication December 14, 2001.

Address reprint requests to Dr. Bahman Anvari, Department of Bioengineering, MS-142, P.O. Box 1892, Rice University, Houston, TX 77251-1892. Tel.: 713-348-5870; Fax: 713-348-5877; E-mail: anvari@rice.edu.

0006-3495/02/03/1386/10 $2.00

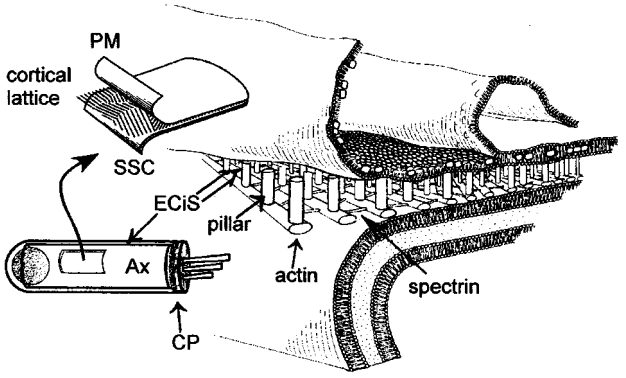

FIGURE 1 Diagram of OHC (*lower left*) with detail of lateral wall components. The OHC lateral wall is a 100-nm-thick trilaminate structure consisting of the PM, CL, and SSC. The CL is composed of cytoskeletal microdomains of parallel actin filaments cross-linked with spectrin. Pillars of ~35 nm in length link the CL to the PM. Axial core (Ax) is the center of the cell, and the extracisternal space (ECiS) is the fluid space between the SSC and the PM, in which lies the CL. The stereocilia are rooted in the cuticular plate (CP) (from Brownell and Popel, 1998).

rameters in the development of nanoscale models to describe and eventually elucidate the mechanism responsible for OHC electromotility.

Several experimental methods including micropipette aspiration, flow chamber, and optical tweezers have been used to study mechanical properties of cell membrane by pulling membrane tethers (Hochmuth et al., 1973; Evans and Hochmuth, 1976a,b; Waugh, 1982a,b; Waugh and Bauserman, 1995; Shao and Hochmuth, 1996; Dai and Sheetz, 1995, 1999). In these studies, the membrane tether was shown to behave as a viscoelastic material and the mechanical properties such as the PM-cytoskeleton separation force, bilayer bending stiffness, and effective membrane viscosity were measured. Single beam gradient laser traps or optical tweezers provide an advanced technique for cellular manipulation and biological force measurements. Using forces generated in the direction of the gradient of light intensity, a particle is pushed near the focal zone of a diffraction-limited spot (Ashkin et al., 1986, Ashkin, 1992). Optical tweezers have been used to manipulate individual cells, organelles, and even single DNA molecules (Ashkin et al., 1987, 1990; Smith et al., 1996). They have also been used to measure a variety of biological forces, including the force of single motor molecules (Block et al., 1990; Kuo and Sheetz, 1993; Finer et al., 1994) and intramolecular force of a single receptor-ligand bond (Zahn and Seeger, 1998). In addition, optical tweezers have been used to form plasma membrane tethers from neuronal growth cone, renal epithelial cells, and fibroblasts with polystyrene or silica microspheres (Dai and Sheetz, 1995, 1999; Raucher and Sheetz, 1999).

Optical tweezers have several advantages compared with other tether formation methods. They allow noninvasive manipulation of cells with great force resolution (~0.1 pN) and can continuously monitor the instantaneous tether force when used in conjunction with a photodetector, which is particularly important in studying membrane mechanical properties dynamically.

In this study, plasma membrane tethers were formed from guinea pig OHCs using optical tweezers. The tether formation force and tether force were measured in both static and dynamic conditions (see Materials and Methods). The apparent PM stiffness and viscosity were estimated from the measured forces and compared with those from other membrane tether studies.

MATERIALS AND METHODS

OHC isolation

Pigmented guinea pigs of either sex weighing 200 to 250 g were decapitated. The temporal bones were removed, and the organ of Corti was isolated from the cochlea. The organ of Corti was incubated in trypsin for ~5 min and transferred to a microwell petri dish (MatTek, Ashland, MA). The petri dish was coated with poly-D-lysine to ensure firm attachment of the OHCs to the coverslip. The OHCs were maintained in a bathing solution consisting of 155 mM NaCl, 4 mM KCl, 1 mM $MgCl_2$, 2 mM $CaCl_2$, and 10 mM HEPES. The solution was adjusted to a pH of 7.2 and an osmolarity of 290 to 300 mOsm/kg. The cells were selected for experimentation if they exhibited a uniformly cylindrical shape, a basally located nucleus, and limited osmotic swelling or Brownian motion in the cytoplasm. All OHCs were used within 4 h after the animal sacrifice.

Experimental setup

The optical tweezers setup used a continuous wave, tunable (650–1100 nm) Titanium-Sapphire laser (Spectra-Physics, Model 3900S, Mountain View, CA) pumped by a 5-W solid state, frequency doubled Nd:YVO_4 laser (Spectra-Physics, Millennia V) (Fig. 2). The Titanium-Sapphire laser was tuned to 830 nm where no or minimal damage to cells has been reported (Liang et al., 1996; Neuman et al., 1999). In our experiments, there was no evidence of damage to the OHCs nor were thermally induced length changes observed. The laser beam was expanded 5 times by a beam expander (Chroma Technology, cwbx-7.0-s-670/1064, Brattleboro, VT) to fill the back aperture of a 100× microscope objective with a numerical aperture of 1.3, thereby achieving a high convergence angle required for strong trapping. An attenuator (Newport, 925B, Irvine, CA) was placed in the beam path to change the light level during experimentation (if needed). The laser beam was directed by two mirrors toward the bottom port of an inverted microscope (Zeiss, Axiovert S100TV, Jena, Germany). A dichroic mirror placed before the bottom port transmitted the laser light into the microscope and reflected the emitted light (<650 nm) from the sample toward a beam splitter, which in turn, transmitted 10% of that light to a CCD camera (DAGE-MTI, CCD100, Michigan City, IN) for image collection, and reflected the remaining 90% to a quadrant photodetector (Hamamatsu, S4349, Somerville, NJ) mounted on a micrometer stage for bead displacement measurements.

The shadow of a 4.5-μm diameter polystyrene trapped bead, which was used as a "handle" to form plasma membrane tethers from the OHC lateral wall, was projected onto the photodetector surface by a 15× eyepiece. The analog photodetector displacement signals resulting from the movement of a trapped bead by the plasma membrane tether were amplified by a circuit and digitized with an A-D converter (Iotech, Wavebook512, Cleveland, OH). The digital signals were subsequently analyzed by a LabView program.

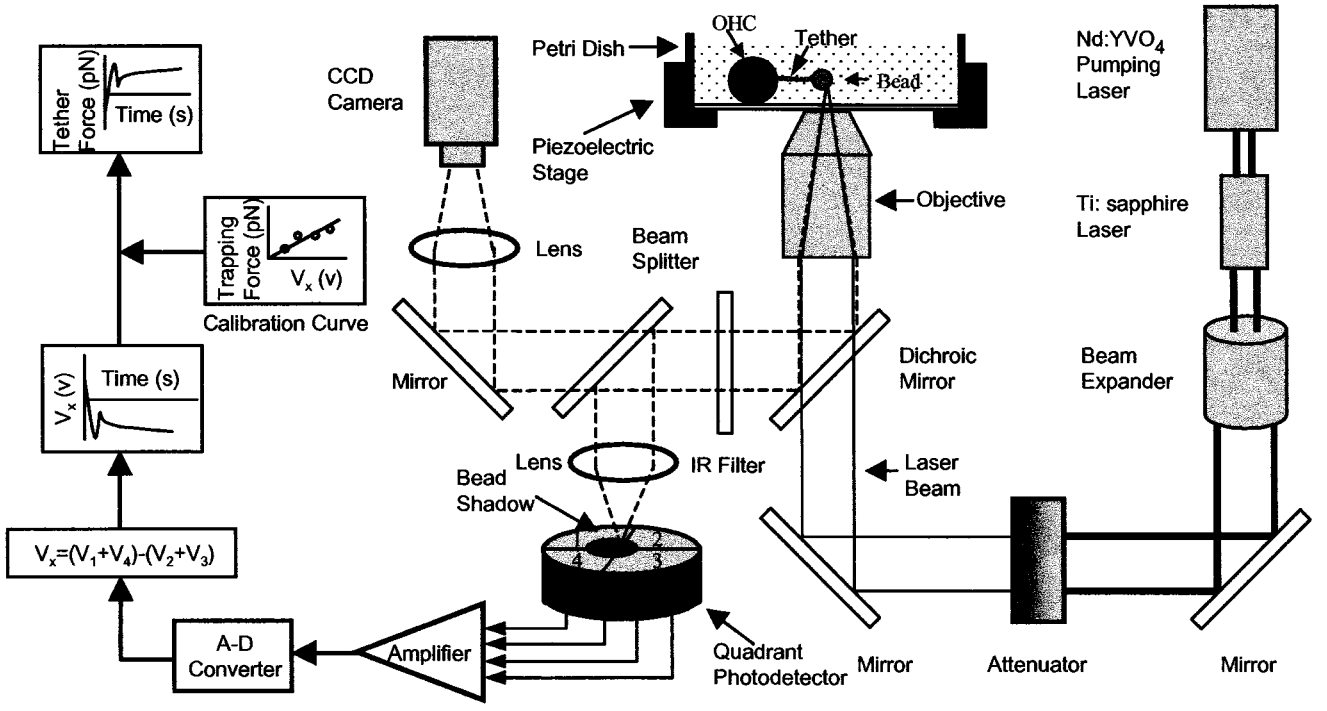

FIGURE 2 Optical tweezers setup. The solid lines represent the laser pathway, and the broken lines represent imaging pathway.

The petri dish containing the OHCs was placed onto a rotation stage mounted onto a piezoelectric translation stage (Physik Instrumente, Model P-527.C3L, Waldbronn, Germany). The piezoelectric stage was positioned on a custom-made manual translation stage for normal microscopic translation. Movement of the piezoelectric stage was controlled by a function generator (Stanford Research Systems, DS345, Sunnyvale, CA). The resolution of the piezoelectric stage was 10 nm in x and y directions and 2 nm in z direction (laser beam propagation direction).

Calibration procedure

Optical tweezers can generate trapping force in both axial (z axis) and transverse (xy plane) directions. In this study, we used the transverse trapping force perpendicular to the laser beam propagation axis. Calibration of the trapping force was performed by passing a solution (by moving the piezoelectric stage) through a trapped bead at a known velocity and calculating the force from the following equation

$$F = \frac{6\pi\eta v r}{1 - \frac{9}{16}\left(\frac{r}{h}\right) + \frac{1}{8}\left(\frac{r}{h}\right)^3 - \frac{45}{256}\left(\frac{r}{h}\right)^4 - \frac{1}{16}\left(\frac{r}{h}\right)^5}, \quad (1)$$

in which η is solution viscosity, v is solution velocity, r is bead radius, and h is the distance between the center of the bead and the coverslip. Eq. 1 is a modified version of Stokes law when a sphere moving in a viscous fluid is very close to the coverslip (Happel and Brenner, 1965).

The transverse trapping force is a function of both laser power and the distance from the trap center. For a given laser power, the bead will eventually escape the trap when the drag force by the moving fluid overcomes the trapping force at a sufficiently high fluid velocity. We refer to the drag force, which is sufficient to release the bead from the trap as the escaping force (F_{es}) and determine it over a range of laser power (P) measured past the microscope objective. Fig. 3 shows the escaping force as a function of laser power for a 4.5-μm polystyrene bead with a refractive index of 1.6 placed at a height of 5 μm from the coverslip. There was a linear relationship between the escaping force and laser power and the trapping stiffness (i.e., the slope of F_{es} versus P) was ~1.3 pN/mW.

During the calibration procedure for the trapping force, the shadow of the trapped bead was projected onto the surface of the quadrant photodetector generating a voltage signal on each of its four quadrants (V_1 through V_4) (Fig. 2). Bead displacement in x direction (corresponding to the direction of fluid flow) was characterized by the voltage difference $V_x = (V_1 + V_4) - (V_2 + V_3)$. For a given laser power, V_x was recorded at different fluid velocities, which corresponded to different trapping forces. In this study, we did the calibration when the pumping laser was set at a maximal output of 5 W, which resulted in laser power of 500 mW after the

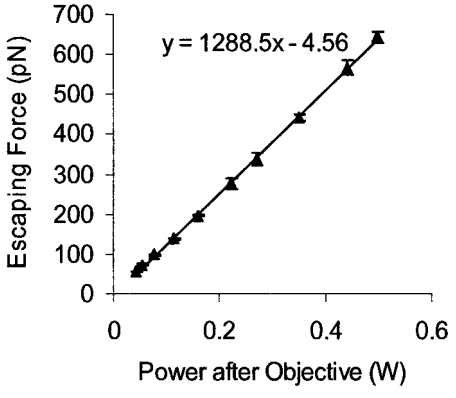

FIGURE 3 Calibration of escaping force as a function of laser power after the microscope objective.

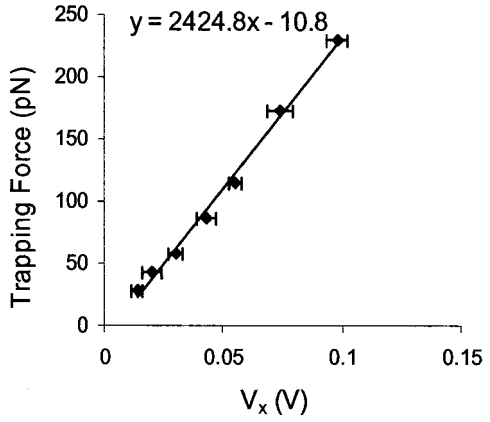

FIGURE 4 Calibration of trapping force as a function of photodetector output voltage, V_x.

microscope objective. The calibration of the trapping force as a function of V_x for 4.5-μm polystyrene bead placed at a height of 5 μm from the coverslip is shown in Fig. 4. The output of each quadrant was initially 0.6 V (in response to the level of microscope illumination) with the bead trapped and in the absence of flow. The light level during tether experiments was kept at the same level as in the calibration procedure.

Tether force measurements

Static force measurements

An OHC (or a supporting Deiters or Hensen cell) that was firmly attached to the coverslip was brought in contact with an optically trapped bead by moving the stage. After a 5-s contact time, the cell was moved away to form a plasma membrane tether. If the laser power was not large enough, the trapping force exerted on the bead could not overcome the attachment force of PM to CL, and as a result the bead would be moved out of the trap by the cell. The laser power was increased in a stepwise fashion by increasing the light transmission through the attenuator, and pulling was repeated until detachment of the bead from the cell was achieved. The presence of PM tether was indicated as the bead rapidly returned back toward the cell wall once the laser light was cutoff. The tether formation force was measured for OHC lateral wall, OHC basal end, and supporting cells (Deiters cells and Hensen cells).

Once a tether was formed, the cell was moved away at a speed of 2 μm/s until the tether was extended to a length ranging between 5 and 20 μm. At a given tether length, laser power was then decreased gradually until the tether force exceeded the strength of the optical trap, causing a rapid return of the bead to the cell wall. Almost all of the measurements were completed within 15 s, and the tethers were pulled to the desired length. We refer to the tether force measured by this method as the static tether force.

Dynamic force measurements

The instantaneous tether force was measured using the quadrant photodetector, which recorded the shadow of the trapped bead projected on its quadrants. After the cell was in physical contact with the trapped bead for 5 s, it was moved away at a constant speed ranging between 0.5 to 4 μm/s. As the piezoelectric stage moved the cell, the photodetector measured the amount of the change in the shadow of the trapped bead, which was induced by displacement of the bead from the trap center. As the tether was elongating and displacing the bead, a continuous curve of V_x against time was obtained. Using this curve together with the trapping force calibration curve (Fig. 4), the instantaneous tether force was measured. Some tethers were pulled at increasing rates during one recording. In such experiments, the cell was initially moved at 0.5 μm/s for 20 s, followed by movements at 1 μm/s for 10 s, 2 μm/s for 7.5 s, and 4 μm/s for 7.5 s. Total displacement for tether-elongated length in these experiments was 65 μm and lasted for 45 s. In several experiments, the tether was pulled and maintained at a constant length for an extended time, allowing for measurements of tether force relaxation.

Tether fluorescence imaging

Inasmuch as tethers from OHC were not visible under normal light microscopy, we labeled OHC plasma membrane with Di-8-ANEPPS (Molecular Probes, D-3167, Eugene, OR), which is a styryl dye that specifically binds to plasma membrane (Oghalai et al., 1998). This dye is a molecule with a nonpolar region that inserts into membranes and a fluorescent polar region. When bound to phospholipid vesicles, Di-8-ANEPPS has absorption/emission maxima of ~ 467/631 nm. It stains OHC plasma membrane very well and does not internalize significantly (Fluhler et al., 1985). The fluorescent dye was excited by the light from a Halogen lamp passing through a band pass filter (480/40 nm) (Chroma Technology, Brattleboro, VT). The fluorescence was filtered through an emission filter (645/75 nm) (Chroma Technology) and imaged by the CCD camera.

RESULTS

Tether fluorescence imaging

A fluorescent image showing the OHC plasma membrane labeled with Di-8-ANEPPS is presented in Fig. 5. The thin strand linking the lateral wall and the bead is PM tether.

Static force measurements

Tether formation force

Average tether formation forces ($\pm$SD) for OHC lateral wall, OHC basal end, Deiters cells, and Hensen cells were 499 $\pm$ 152 (n = 44), 142 $\pm$ 49 (n = 14), 146 $\pm$ 44 (n = 13), and 116 $\pm$ 15 (n = 13) pN, respectively (Fig. 6). The tether formation force for the basal end was ~28% of that for the lateral wall.

Static tether force

The static measurements of the tether force as a function of tether length for OHC lateral wall and OHC basal end are shown in Fig. 7. The tether force for the lateral wall was larger than that for the basal end, but increased with tether length for both the lateral wall and the basal end. The tether stiffness estimated from the slope of tether force versus tether length was 3.71 pN/μm for the lateral wall and 4.57 pN/μm for the basal end.

Dynamic force measurements

A typical dynamic tether force measurement is shown in Fig. 8. In this measurement, the cell was moved 40 μm

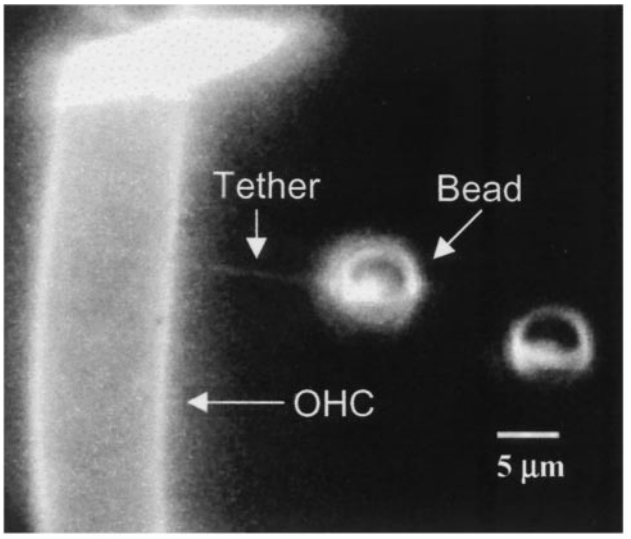

FIGURE 5 Fluorescent image of the apical end of an outer hair cell with a plasma membrane tether.

away from the bead at a pulling rate (ν) of 1 μm/s. Note that the force was negative before the beginning of pulling because the cell pushed the bead in the direction opposite to that of the stage movement. Membrane tether was formed when the cell was moved ~3.4 μm away, and the tether formation force was ~300 pN. Once the tether was formed, the tether force dropped to ~100 pN, and gradually increased to a steady-state force (F_s) of 115 pN where it remained approximately constant with increased tether length.

Dynamic tether force measurements for the lateral wall plasma membrane were made at pulling rates of 0.5, 1, 2, and 4 μm/s. We observed that the steady-state force tended to become larger with increased pulling rates but was quite variable among different cells subject to the same pulling rate. To eliminate the large variability in the response of

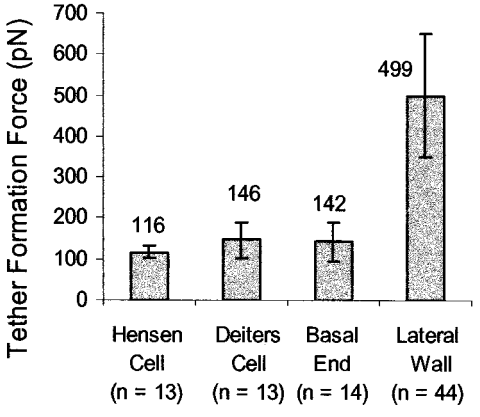

FIGURE 6 Tether formation forces for Hensen cells, Deiters cells, OHC basal end, and OHC lateral wall.

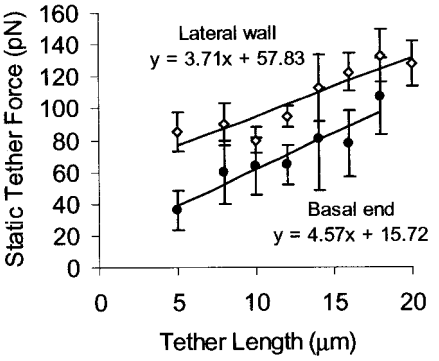

FIGURE 7 Static tether force as a function of tether length for OHC lateral wall and basal end.

different cells, we changed the pulling rate on the same tether (Fig. 9).

In Fig. 9 *A*, the tether force dropped from 290 to 100 pN once the tether was formed, increased to 150 pN, and dropped again to 10 pN. This type of response may be due to additional membrane pulled off from the cell after the initial tether formation. Fig. 9 *A* shows a clear trend in that the tether force began to increase when pulling rate was increased and gradually reached a steady-state value at that pulling rate.

We fit the data for different pulling rates to exponential functions and obtained the steady-state (asymptotic) tether force for each pulling rate. Fig. 9 *B* shows the curve fitting of data for the pulling rate of 1 μm/s. Fig. 9 *C* shows the steady-state tether forces at different pulling rates for the tether shown in Fig. 9 *A*. In some of the four-speed pulling experiments, the tether broke before it reached a full length of 65 μm. These recordings were not used in estimating the slope of the F_s–ν curve. Ten full-length tethers were obtained using the four-speed pulling protocol and the slopes of F_s–ν curve were in the range of 15 to 33 pN·s/μm. The average tether formation force was 492 pN for these 10

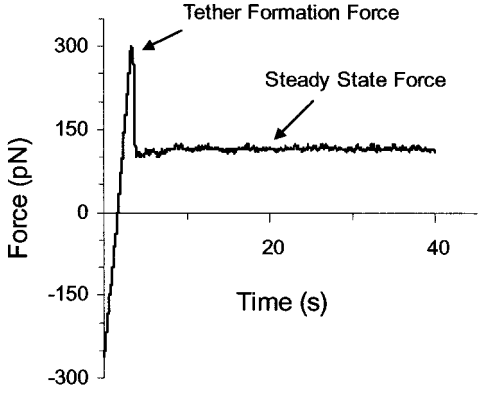

FIGURE 8 Dynamic measurement of tether force as a function of time.

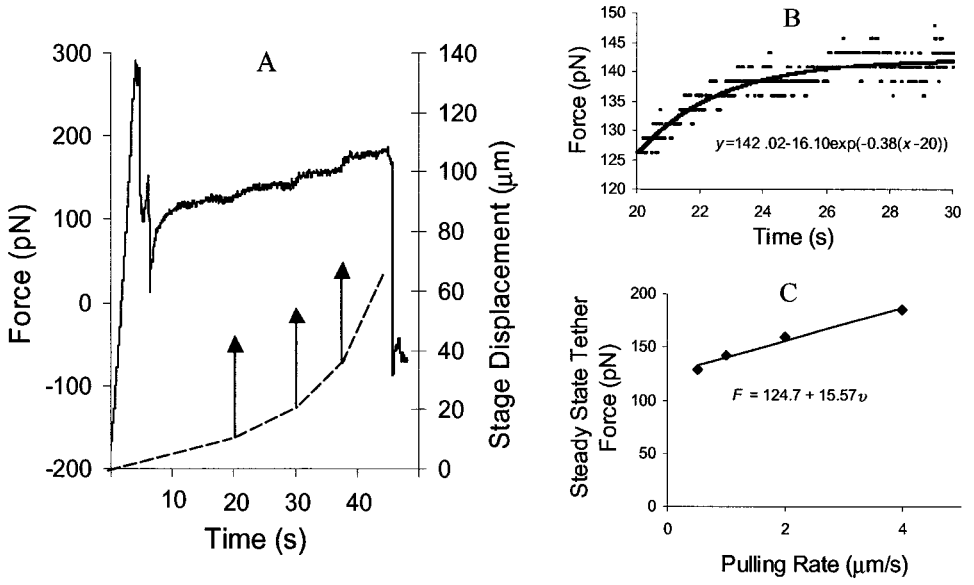

FIGURE 9 (*A*) Dynamic tether force as a function of time from a single tether at four different pulling rates (0.5, 1, 2, and 4 μm/s). The broken line represents the stage displacement for different pulling rates, and the continuous line represents the tether force during pulling. The arrows mark the transitions from a lower pulling rate to a higher pulling rate. In this measurement, the cell was initially moved at 0.5 μm/s for 20 s, followed by movements at 1 μm/s for 10 s, 2 μm/s for 7.5 s, and 4 μm/s for 7.5 s. Total displacement for tether elongated-length was 65 μm and lasted for 45 s. (*B*) Data for pulling rate of 1 μm/s, has been fit to an exponential curve, the correlation coefficient r^2 was 0.824 for this pulling rate and >0.650 for all pulling rates. (*C*) Steady-state tether force as a function of pulling rates for the tether shown in *A*. Data represent the steady-state (asymptotic) force determined from the exponential curve fitting as in *B*. The slope of the fitted line is 15.57 pN·s/μm (r^2 = 0.977).

tethers, and the value was consistent with that (499 pN) obtained from static measurements.

We also did force relaxation measurements in which the tether was pulled and maintained at a constant length for an extended time. One such measurement is shown in Fig. 10. In this measurement the tether was pulled to 10 μm at 0.5 μm/s and maintained at that length. The upper panel shows the entire procedure including tether formation, pulling, and relaxation. The lower panel shows the recording from the moment that tether length reached 10 μm to the moment that tether force reached equilibrium. This cell exhibited a relaxation time constant of 50 s and an equilibrium force of 60 pN. The two spikes on the relaxation curve in the upper panel are due to debris entering the optical trap.

DISCUSSION

Optical tweezers have been used to characterize the mechanical properties of the cell membrane by pulling plasma membrane tethers with microspheres (Dai and Sheetz, 1995, 1999; Raucher and Sheetz, 1999). Most of these studies were performed on membranes without cytoskeleton support (cell bleb membrane) or with very simple cytoskeleton (neuronal growth cone and fibroblast). Little is known about the mechanical properties of cell membrane of more complex cells with extensive cytoskeleton support (such as outer hair cells). With the high laser power (500 mW at the trapping plane) used in our optical tweezers system, we have achieved trapping forces greater than 600 pN, which enables investigations of the OHC lateral wall.

Previous studies have demonstrated that the membrane tether contains only plasma membrane so the tether formation involves separating the plasma membrane from the underlying cytoskeleton. In this study we measured the tether formation force from the lateral wall and the basal end of OHC as well as its supporting cells (Deiters cells and Hensen cells). The force required to form a tether was significantly higher for the lateral wall (499 pN in static measurements and 492 pN in dynamic measurements) than for the basal end (142 pN), Deiters cells (146 pN), and Hensen cells (116 pN). The larger value of the force required to pull tethers from the lateral wall reflects the influence of the OHC cortical lattice. The lateral wall plasma membrane is attached to the cortical lattice, which is absent in the basal end of OHC and supporting cells. The large value of the tether formation force is consistent with micropipette aspiration experiments on the OHC. Greater negative pressures were required to deform the OHC lateral wall than other cell types (Sit et al., 1997) and even larger pressures to detach the plasma membrane (Oghalai et al., 1998).

Other investigators have measured the tether formation force for a variety of cell types using optical tweezers as well as micropipette aspiration and microcantilever tech-

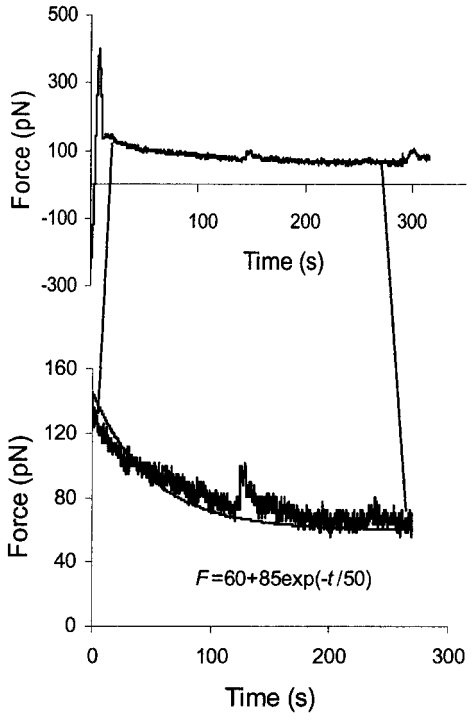

FIGURE 10 Tether force as a function of time showing force relaxation.

niques. The respective values for a leukemic rat cell (Dai and Sheetz, 1998), red blood cells (Waugh and Bauserman, 1995), neutrophils (Shao and Hochmuth, 1996), chick fibroblasts (Raucher and Sheetz, 1999), and neuronal growth cones (Hochmuth et al., 1996) have been reported as 70, 50, 45, 35, and 8 pN. It is pointed out (Hwang and Waugh, 1997; Hochmuth et al., 1996) that the tether force at zero tether growth rate (F_0) extrapolated from a tether force versus tether growth rate curve was the minimal force to form a tether. This is probably true for pure lipid vesicles or some cell types where the plasma membrane is not firmly attached to the cytoskeleton.

In our tether experiments on OHC lateral wall, the tether formation force was much larger than the force at zero pulling rate. The most likely reason for this difference is that the plasma membrane of the OHC lateral wall is firmly attached to the cytoskeleton by the pillars. The work required to detach the PM from the cytoskeleton (probably by breaking the pillars) is greater than for other cells with less extensive attachments of the PM to the cytoskeleton. Once a tether is formed, less force is required to elongate it than is required to form it. In cells with extensive cytoskeletal support (e.g., the OHC), an irreversible component of the work in tether formation may give rise to differences between the measured tether formation force and the extrapolated value to zero tether growth rate. We observed that in some cases after a tether was formed and stretched, the bead returned toward the cell wall but not back to its original position once the laser power was cutoff. Instead the bead exhibited some movement with a loose tether connected to the cell wall. Sometimes although the bead returned to its original position on the cell wall where the tether was formed, less force was needed to pull the tether again than that required to form the tether the first time. These observations suggest that the tether formation process from OHC involves an irreversible component of work, which gives a tether formation force larger than the tether force at zero tether growth rate.

The influence of CL on lateral wall mechanics as opposed to pure PM mechanics has been observed during micropipette aspiration experiments on the OHC. The stiffness parameter calculated for deformation of the intact lateral wall (Sit et al., 1997; Spector et al., 1998a,b) is approximately four times that measured once the plasma membrane is detached (Oghalai et al., 1998).

We measured the static tether force for tether lengths ranging between 5 and 20 μm from the lateral wall and basal end of OHC. The tether stiffness estimated from the slope of tether force versus tether length was 3.71 pN/μm for the lateral wall and 4.57 pN/μm for the basal end. The difference in tether stiffness may be due to differences in the lipid composition of the PM of the lateral wall and the basal end. A previous study has demonstrated that more cholesterol is present in the basal end than in the lateral wall (Nguyen and Brownell, 1998).

The results of the static tether force as a function of tether length (Fig. 7) appear to contradict those obtained by dynamic measurements (Fig. 8) in that the former demonstrate that the force increases with tether length, whereas the latter shows that the force approaches a steady-state value. The discrete static values correspond to the average force obtained from different tethers, whereas the values obtained in the dynamic measurements are for the same tether. Additionally, the static measurements lack the viscous component of the force value, which is present in dynamic measurements. Last, the force relaxation, which can take place during static measurements, is absent during dynamic measurements. From the relaxation experiments, we observed that the force relaxed immediately after the pulling was stopped. In the process of decreasing the laser power during static measurements, the bead moved toward the cell so that the force relaxed even more. As a result, the static tether force should be smaller than dynamic tether force, and this is what we observed.

An analysis of the tether formation process is important because it leads to further understanding of the plasma membrane-cytoskeleton interface and is particularly relevant to the processes of secretion and signaling (Hochmuth et al., 1996). A thermodynamic analysis of the tether formation process was presented by Hochmuth and applied to experimental studies of tether formation from different cell types such as neuronal growth cones. The dissipation of energy during tether formation comes from three sources:

1) an increase in bending energy as the PM moves from the cell body to the cylindrical tether with a constant curvature, 2) the energy to separate the PM from the cytoskeleton, and 3) the energy to overcome the viscous resistance within the system. Tether force at zero pulling rate (F_0) is the sum of the forces to overcome PM bending and separate the PM from the cytoskeleton. The resistance of the membrane to bending depends both on the intrinsic stiffness of the individual monolayer in a local region (local bending) and on the curvature-induced expansion or compression of the monolayers relative to each other (nonlocal bending) (Waugh and Hochmuth, 1987; Bo and Waugh, 1989; Waugh et al., 1992). Three sources of viscosities are postulated to account for the viscous dissipation during tether formation: 1) surface viscosity in each monolayer ($\eta_m/2$); 2) viscous slip between each of the monolayers (η_{si}); and 3) the viscous slip of the (inner monolayer) membrane over the cytoskeleton (η_{sc}). The effective viscosity (η_{eff}), representing the overall viscosity from the three viscous sources, can be written as

$$\eta_{eff} = (F - F_0)/2\pi V_t , \qquad (2)$$

in which V_t is the tether growth rate.

Membrane viscosity is an important factor in determining the rate at which the membrane can undergo deformation and influences the rate at which particles can diffuse in the plane of the surface (Waugh, 1982b). In this study, we estimated the effective membrane viscosity of OHC from the slope of $F_s - \nu$ curve by measuring the steady-state tether force at different pulling rates. The slopes from these $F_s - \nu$ curves were in the range of 15 to 33 pN·s/μm. The effective viscosity values using Eq. 2 were calculated in the range of 2.39 to 5.25 pN·s.μm, which are similar to the value for neutrophils ($\approx$1.8 pN·s/μm) (Shao and Hochmuth, 1996), but considerably less than the value for red blood cells ($\approx$34 pN·s/μm) (Hwang and Waugh, 1997).

The values of membrane surface viscosity are reported in the range of 5 to 13 $\times$ 10^{-3} pN·s/μm for vesicles from egg phosphatidylcholine diluted in hexane (Waugh, 1982a,b). Membrane surface viscosity for a lipid membrane is also reported to have a value of 0.001 pN·s/μm (Evans and Yeung, 1994). The effective viscosity, calculated using Eq. 2 is 0.071 pN·s/μm for bilayer vesicles made from a 1:1 mixture of bovine brain sphingomyelin and cholesterol (Evans and Yeung, 1994) and 0.009 pN·s/μm for vesicles made from 1-stearoyl-2-oleoyl-*sn*-glycero-3-phosphocholine (Yeung, 1994). The effective viscosity is 0.137 pN·s/μm for neuronal growth cones (Hochmuth et al., 1996). Because the effective viscosity of the phospholipid vesicles is approximately one to two orders of magnitude smaller than those of OHC, we can conclude that the membrane viscosity (η_m) and viscous slip between each of the monolayers (η_{si}) are much smaller than the viscous slip of the (inner monolayer) membrane over the cytoskeleton (η_{sc}) and contribute little to the effective viscosity of OHC lateral wall. The effective viscosity of OHC lateral wall is approximately one order larger than that of neuronal growth cones. This may be due to the additional viscous interactions between the plasma membrane lipids and cytoskeletal anchored proteins.

In our setup, the laser was tuned to 830 nm, a wavelength that is shown to only cause minimal damage to the *Escherichia coli* within the optical trap (Neuman et al., 1999). We have observed that the optical trap can damage the red blood cells if the power is sufficiently high (>300 mW); however, there was no observable damage to OHCs even with the maximal power (500 mW). There may still be a possibility that the laser can cause local heating on the membrane attached to the trapped beads.

When pulling tethers, the drag force induced by the surrounding medium would affect the force measurements. With the low pulling rates of several microns per second applied in our studies, the fluid drag force on the bead was less than 1 pN, which is negligible compared with the much larger tether force. The trap could also exert some force directly on the tethers. Because the tether has a smaller diameter and is further separated from the trap compared to the bead, it is unlikely that the direct force on the tether is more than 20% of that on the bead (Dai and Sheetz, 1995).

Amphipathic drugs such as salicylate and chlorpromazine can alter membrane curvature by preferentially partitioning into either the outer or inner leaflet of the phospholipid bilayer, selectively increasing the leaflet's surface area. Salicylate interacts with the PM of red blood cell resulting in an outward membrane buckling (crenation), whereas chlorpromazine bends the red blood cell membrane inward (cupping) (Sheetz and Singer, 1974; Sheetz et al., 1976). Agents that alter membrane curvature would be expected to affect the mechanical properties of the OHC plasma membrane as observed with micropipette aspiration (Morimoto et al., 2002). In our future experiments, we will study the effects of salicylate and chlorpromazine on tether formation from the lateral wall of the outer hair cells using optical tweezers.

In summary, optical tweezers were used to characterize the mechanical properties of the outer hair cell plasma membrane by pulling tethers with 4.5-μm polystyrene beads. A greater force was required for tether formations from OHC lateral wall (499 $\pm$ 152 pN) than from OHC basal end (142 $\pm$ 49 pN). The difference in the force required to pull tethers is consistent with an extensive cytoskeletal framework associated with the lateral wall. The apparent PM stiffness, estimated under the static conditions by measuring tether force at different tether length, was 3.71 pN/μm for OHC lateral wall and 4.57 pN/μm for OHC basal end. The effective membrane viscosity was estimated in the range of 2.39 to 5.25 pN·s/μm. The viscous force most likely results from the viscous interactions between plasma membrane lipids and cytoskeletal anchored proteins.

This work was supported by grant from the National Institute on Deafness and other Communication Disorders (2R01-DC02775-06). We thank Drs. R. M. Raphael, A. A. Spector, and A. S. Popel for their valuable comments, and Dr. H-B. Zhao and C. Shope for their help on OHC isolation and fluorescence imaging.

REFERENCES

Arima, T., A. Kuraoka, R. Toriya, Y. Shibata, and T. Uemura. 1991. Quick-freeze, deep-etch visualization of the "cytoskeletal spring" of cochlear outer hair cells. *Cell Tissue Res.* 263:91–97.

Ashkin, A. 1992. Forces of a single-beam gradient laser trap on a dielectric sphere in the ray optics regime. *Biophys. J.* 61:569–582.

Ashkin, A., J. M. Dziedzic, J. E. Bjorkholm, and S. Chu. 1986. Observations of a single-beam gradient force optical trap for dielectric particles. *Opt. Lett.* 11:287–289.

Ashkin, A., J. M. Dziedzic, and T. Yamane. 1987. Optical trapping and manipulation of single cells using infrared laser beams. *Nature.* 330: 769–772.

Ashkin, A., K. Schutze, J. M. Dziedzic, U. Euteneuer, and M. Schliwa. 1990. Force generation of organelle transport measured in vivo by an infrared laser trap. *Nature.* 348:346–348.

Ashmore, J. F. 1987. A fast motile response in guinea-pig outer hair cells: the cellular basis for the cochlear amplifier. *J. Physiol.* 388:323–348.

Block, S. M., L. S. B. Goldstein, and B. J. Schnapp. 1990. Bead movement by single kinesin molecules studied with optical tweezers. *Nature.* 348:348–352.

Bo, L., and R. E. Waugh. 1989. Determination of bilayer membrane bending stiffness by tether formation from giant, thin-walled vesicles. *Biophys. J.* 55:509–517.

Brownell, W. E. 1990. Outer hair cell electromotility and otoacoustic emissions. *Ear Hear.* 11:82–92.

Brownell, W. E., C. R. Bader, D. Bertrand, and Y. Ribaupierre. 1985. Evoked mechanical responses of isolated cochlear outer hair cells. *Science.* 227:194–196.

Brownell, W. E., and A. S. Popel. 1998. Electrical and mechanical anatomy of the outer hair cell. *In* Psychophysical and Physiological Advances in Hearing. A.R. Palmer, A. Rees, A.Q. Summerfield, and R. Meddis, editors. Whurr Publishers, London. 89–96.

Brownell, W. E., A. A. Spector, R. M. Raphael, and A. S. Popel. 2001. Micro- and nanomechanics of the cochlear outer hair cell. *Annu. Rev. Biomed. Eng.* 3:169–194.

Dai, J., and M. P. Sheetz. 1995. Mechanical properties of neuronal growth cone membranes studied by tether formation with laser optical tweezers. *Biophys. J.* 68:988–996.

Dai, J., and M. P. Sheetz. 1998. Cell membrane mechanics. *In* Methods in Cell Biology. Vol. 55, Laser Tweezers in Cell Biology. M.P. Sheetz, editor. Academic Press, San Diego, CA. 157–171.

Dai, J., and M. P. Sheetz. 1999. Membrane tether formation from blebbing cells. *Biophys. J.* 77:3363–3370.

Dallos, P., and M. E. Corey. 1991. The role of outer hair cell motility in cochlear tuning. *Curr. Opin. Neurobiol.* 1:215–220.

Dieler, R., W. E. Shehata-Dieler, and W. E. Brownell. 1991. Concomitant salicylate-induced alterations of outer hair cells. *J. Neurocytol.* 20: 637–653.

Evans, E. A., and R. M. Hochmuth. 1976a. Membrane viscoelasticity. *Biophys. J.* 16:1–12.

Evans, E. A., and R. M. Hochmuth. 1976b. Membrane viscoplastic flow. *Biophys. J.* 16:13–26.

Evans, E. A., and A. Yeung. 1994. Hidden dynamics in rapid changes of bilayer shape. *Chem. Phys. Lipids.* 73:39–56.

Finer, J. T., R. M. Simmons, and J. A. Spudich. 1994. Single myosin molecule mechanics: piconewton forces and nanometer steps. *Nature.* 368:113–119.

Fluhler, E., V. G. Burnham, and L. M. Loew. 1985. Spectra, membrane binding, and potentiometric responses of new charge shift probes. *Biochemistry.* 24:5749–5755.

Happel, J., and H. Brenner. 1965. Low Reynolds Number Hydrodynamics with Special Applications to Particulate Media. Prentice-Hall, Englewood Cliffs, NJ. 327.

Hochmuth, R. M., N. Mohandas, and P. L. Blackshear. 1973. Measurement of the elastic modulus for red cell membrane using a fluid mechanical technique. *Biophys. J.* 13:747–762.

Hochmuth, R. M., J. Shao, J. Dai, and M. P. Sheetz. 1996. Deformation and flow of membrane into tethers extracted from neuronal growth cones. *Biophys. J.* 70:358–369.

Holley, M. C. 1992. Structure of the cortical cytoskeleton in mammalian outer hair cells. *J. Cell Sci.* 102:569–580.

Holley, M. C. 1996. Outer hair cell motility. *In* The Cochlea. P. Dallos, A.N. Proper, and R.R. Fay, editors. Spring-Verlag, New York. 386–434.

Hwang, W. C., and R. E. Waugh. 1997. Energy of dissociation of lipid bilayer from the membrane skeleton of red blood cells. *Biophys. J.* 72:2669–2678.

Isawa, K. H. 1993. Effect of stress on the membrane capacitance of the auditory outer hair cell. *Biophys. J.* 65:492–498.

Isawa, K. H. 1994. A membrane motor model for the fast motility of the outer hair cell. *J. Acoust. Soc. Am.* 96:2216–2224.

Kuo, S. C., and M. P. Sheetz. 1993. Force of single kinesin molecules measured with optical tweezers. *Science.* 260:232–243.

Liang, H., K. T. Vu, P. Krishnan, T. C. Trang, D. Shin, S. Kimel, and M. W. Berns. 1996. Wavelength dependence of cell cloning efficiency after optical trapping. *Biophys. J.* 70:1529–1533.

Morimoto, N., R. M. Raphael, A. Nygren, and W. E. Brownell. 2002. Excess plasma membrane and effects of ionic amphipaths on the mechanics of the outer hair cell lateral wall. *Am. J. Physiol.* 282: in press.

Neuman, K. C., E. H. Chadd, G. F. Liou, K. Bergman, and S. M. Block. 1999. Characterization of photodamage to *Escherichia coli* in optical traps. *Biophys. J.* 77:2856–2863.

Nguyen, T. V., and W. E. Brownell. 1998. Contribution of membrane cholesterol to outer hair cell lateral wall stiffness. *Otolaryngol. Head Neck Surg.* 119:14–20.

Oghalai, J. S., A. A. Patel, T. Nakagawa, and W. E. Brownell. 1998. Fluorescence-imaged microdeformation of the outer hair cell lateral wall. *J. Neurosci.* 18:48–58.

Pollice, P. A., and W. E. Brownell. 1993. Characterization of the outer hair cell's lateral membrane. *Hear. Res.* 70:187–196.

Raphael, R. M., A. S. Popel, and W. E. Brownell. 2000. A membrane bending model of outer hair cell electromotility. *Biophys. J.* 78: 2844–2862.

Raucher, D., and M. P. Sheetz. 1999. Characteristics of a membrane reservoir buffering membrane tension. *Biophys. J.* 77:1992–2002.

Santos-Sacchi, J. 1993. Harmonics of outer hair cell motility. *Biophys. J.* 65:2217–2227.

Shao, J., and R. M. Hochmuth. 1996. Micropipette suction for measuring piconewton forces of adhesion and tether formation from neutrophil membranes. *Biophys. J.* 71:2892–2901.

Sheetz, M. P., R. G. Painter, and S. J. Singer. 1976. Biological membranes as bilayer couples: III. Compensatory shape changes induced in membranes. *J. Cell Biol.* 70:193–203.

Sheetz, M. P., and S. J. Singer. 1974. Biological membranes as bilayer couples: a molecular mechanism of drug-erythrocyte interactions. *Proc. Natl. Acad. Sci. U.S.A.* 71:4457–4461.

Sit, P. S., A. A. Spector, A. J. Lue, A. S. Popel, and W. E. Brownell. 1997. Micropipette aspiration on the outer hair cell lateral wall. *Biophys. J.* 72:2812–2819.

Smith, S. B., Y. Cui, and C. Bustamante. 1996. Overstretching B-DNA: the elastic response of individual double-stranded and single-stranded DNA molecules. *Science.* 271:795–799.

Spector, A. A., W. E. Brownell, and A. S. Popel. 1998a. Analysis of the micropipette experiment with the anisotropic outer hair cell wall. *J. Acoust. Soc. Am.* 103:1001–1006.

Spector, A. A., W. E. Brownell, and A. S. Popel. 1998b. Estimation of elastic moduli and bending stiffness of the anisotropic outer hair cell wall. *J. Acoust. Soc. Am.* 103:1007–1011.

Waugh, R. E. 1982a. Surface viscosity measurements from large bilayer vesicle tether formation: I. Analysis. *Biophys. J.* 38:19–27.

Waugh, R. E. 1982b. Surface viscosity measurements from large bilayer vesicle tether formation: II. Experiments. *Biophys. J.* 38:29–37.

Waugh, R. E., and R. G. Bauserman. 1995. Physical measurements of bilayer-skeletal separation forces. *Ann. Biomed. Eng.* 23:308–321.

Waugh, R. E., and R. M. Hochmuth. 1987. Mechanical equilibrium of thick, hollow, liquid membrane cylinders. *Biophys. J.* 52:391–400.

Waugh, R. E., J. Song, S. Svetina, and B. Zeks. 1992. Local and nonlocal curvature elasticity in bilayer membranes by tether formation from lecithin vesicles. *Biophys. J.* 61:974–982.

Yeung, A. 1994. Mechanics of inter-monolayer coupling in fluid aurfactant bilayers. PhD Thesis. Department of Physics, University of British Columbia, Canada.

Zahn, M., and S. Seeger. 1998. Optical tweezers in pharmacology. *Cell. Mol. Biol.* 44:747–761.